Whole brain mapping of glutamate distribution in adult and old primates at 11.7T

Clément Garin, Nachiket Nadkarni, Jérémy Pépin, Julien Flament, Marc Dhenain

Whole brain mapping of glutamate distribution in adult and old primates at 11.7T

Clément M. Garin[1,2], Nachiket A. Nadkarni[1,2], Jérémy Pépin[1,2], Julien Flament[1,2,$], Marc Dhenain[1,2,$,*]

[1] Université Paris-Saclay, CEA, CNRS, Laboratoire des Maladies Neurodégénératives, 18 Route du Panorama, F-92265 Fontenay-aux-Roses, France.
[2] Commissariat à l'Energie Atomique et aux Energies Alternatives (CEA), Direction de la Recherche Fondamentale (DRF), Institut François Jacob, MIRCen, 18 Route du Panorama, F-92265 Fontenay-aux-Roses, France

$: These two authors participated equally to the work

Correspondence

Marc Dhenain
MIRCen, UMR CEA-CNRS 9199
18 Route du Panorama
92 265 Fontenay-aux-Roses CEDEX
France
Tel: +33 1 46 54 81 92; Fax: +33 1 46 54 84 51
email: Marc.Dhenain@cea.fr

Abstract

Glutamate is the amino acid with the highest cerebral concentration. It plays a central role in brain metabolism. It is also the principal excitatory neurotransmitter in the brain and is involved in multiple cognitive functions. Alterations of the glutamatergic system may contribute to the pathophysiology of many neurological disorders. For example, changes of glutamate availability are reported in rodents and humans during Alzheimer's and Huntington's diseases, epilepsy as well as during aging.

Most studies evaluating cerebral glutamate have used invasive or spectroscopy approaches focusing on specific brain areas. Chemical Exchange Saturation Transfer imaging of glutamate (gluCEST) is a recently developed imaging technique that can be used to study relative changes in glutamate distribution in the entire brain with higher sensitivity and at higher resolution than previous techniques. It thus has strong potential clinical applications to assess glutamate changes in the brain. High field is a key condition to perform gluCEST images with a meaningful signal to noise ratio. Thus, even if some studies started to evaluate gluCEST in humans, most studies focused on rodent models that can be imaged at high magnetic field.

In particular, systematic characterization of gluCEST contrast distribution throughout the whole brain has never been performed in humans or non-human primates. Here, we characterized for the first time the distribution of the gluCEST contrast in the whole brain and in large-scale networks of mouse lemur primates at 11.7 Tesla. Because of its small size, this primate can be imaged in high magnetic field systems. It is widely studied as a model of cerebral aging or Alzheimer's disease. We observed high gluCEST contrast in cerebral regions such as the nucleus accumbens, septum, basal forebrain, cortical areas 24 and 25. Age-related alterations of this biomarker were detected in the nucleus accumbens, septum, basal forebrain, globus pallidus, hypophysis, cortical areas 24, 21, 6 and in olfactory bulbs. An age-related gluCEST contrast decrease was also detected in specific neuronal networks, such as fronto-temporal and evaluative limbic networks. These results outline regional differences of gluCEST contrast and strengthen its potential to provide new biomarkers of cerebral function in primates.

Graphical abstract

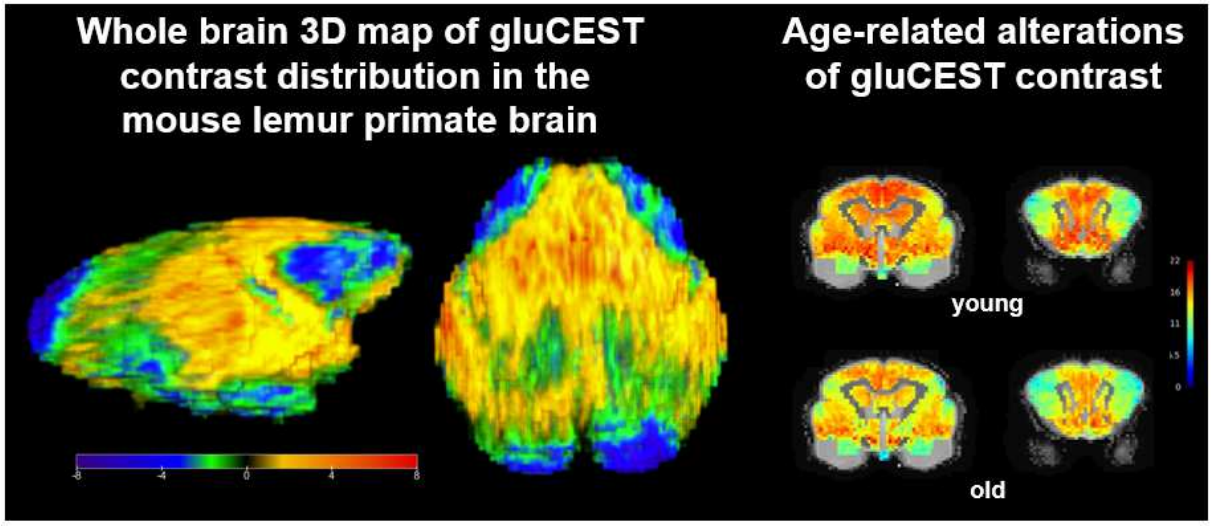

Highlights

- Glutamate, a critical amino acid for the brain, can be detected by gluCEST imaging.
- Whole brain gluCEST maps were recorded at high field (11.7T) MRI in a primate.
- Regional differences of gluCEST contrast strongly reflect glutamate pathways
- gluCEST imaging highlights regional age-related alterations.
- gluCEST imaging highlights age-related alterations in large-scale networks.

Keywords

Aging, Cerebral network, GluCEST, Glutamate, mouse lemur

Significance Statement

In vivo imaging is a primary tool for assessing and diagnosing pathophysiological cerebral changes. Novel techniques are continuously implemented to explore new aspects of cerebral function. Glutamate plays a central role in brain metabolism. It is involved in multiple cognitive functions and is the principal excitatory neurotransmitter in the brain. Chemical Exchange Saturation Transfer imaging of glutamate (gluCEST) is a novel technique with potential clinical applications to assess glutamate changes in the brain. This study characterized for the first time in a non-human primate, a whole brain map of gluCEST contrast. We observed regional differences of gluCEST contrast, age-related alterations occurring in different regions and large-scale networks. These results outline regional differences of gluCEST contrast and strengthen its potential to provide new biomarkers of cerebral function in primates.

1. Introduction

Over the last century, human life expectancy has dramatically increased and the number of aged individuals is still rising. This trend results in the increased incidence of cerebral alterations that induce neurodegenerative diseases or mild cognitive/motor impairments, which limit facets of daily living. This leads to a continuous demand for strengthening the research effort on mechanisms responsible for cerebral aging, and on therapies to prevent age-related diseases.

Glutamate is an essential amino acid of the brain metabolism and has the highest amino acid concentration of the brain (≈10 mmol/kg) (Greenamyre, 1986; Niciu et al., 2012). It is central to several metabolic pathways related to energy metabolism and oxidative stress (Sonnewald, 2014; Zhou and Danbolt, 2014). It is also the principal excitatory neurotransmitter in the brain and is involved in multiple cognitive functions. In normal conditions, glutamate is mostly located in the neurons (Cooper and Jeitner, 2016), neurotransmission being governed by few micromolar of extracellular glutamate.

Given, the importance of glutamate for the brain, *in vivo* markers for brain glutamate can have strong clinical application to provide better diagnostics and aid in the development of early therapeutic intervention. Many studies of glutamate concentrations were based on magnetic resonance spectroscopy. As examples, such studies highlighted age-related reduction of cerebral glutamate concentration in humans during aging (Roalf et al., 2020; Sailasuta et al., 2008) and these changes were associated with cognitive declines (Zahr et al., 2008). Changes of glutamate are also reported in neurodegenerative pathology as Alzheimer's disease (Kirvell et al., 2006). One limitation of this method is that measurements are confined to relatively large voxels. Recent developments of Chemical Exchange Saturation Transfer of glutamate (gluCEST) imaging allow the mapping of relative levels of glutamate concentration in the whole brain (Cai et al., 2012; Carrillo-de Sauvage et al., 2015). CEST has been proposed to indirectly detect brain metabolites/macromolecules with labile protons (-OH, -NH_2, -NH). Exchangeable protons of a metabolite (*e.g.*, -NH_2 amine group of glutamate) exhibit a resonance frequency that is shifted relative to bulk proton frequency. Likewise, exchangeable protons can be saturated using a frequency-selective pulse optimised to saturate amine groups of glutamate, leading to a proportional decrease of water signal due to magnetization exchange (Roalf et al., 2017). Thus, the change in free water magnetization, while selectively saturating

the exchangeable protons of the metabolite, represents an indirect measurement of the metabolite content and the specific glutamate contribution can be estimated by quantifying asymmetrical magnetization transfer ratio (Liu et al., 2010). Approximately 70% of gluCEST value has been shown to be due to glutamate, based on theoretical as well as experimental studies (Bagga et al., 2018; Cai et al., 2012).

High field is a key condition to perform gluCEST images with a meaningful signal to noise ratio. Thus, even if some studies started to evaluate gluCEST in humans (Nanga et al., 2018), most studies focused on rodent models that can be imaged at a high magnetic field. Studies in these animals have shown that gluCEST can characterize glutamate alterations related to Alzheimer's (Haris et al., 2013) or Huntington's disease (Pepin et al., 2016) in mouse models. To our knowledge, systematic characterization of gluCEST contrast distribution has never been performed in humans or non-human primates. Here, we characterized for the first time the distribution of gluCEST contrast throughout the entire brain and in large-scale networks of mouse lemur primates (*Microcebus murinus*) at 11.7 Tesla.

This primate is characterized by its small size (typical length 12cm, 60-120g weight) and can thus easily be imaged with small bore high field MRI. As with all non-human primates, it shares several genetic, physiological, and anatomical similarities with humans. It has a decade-long lifespan (Pifferi et al., 2018) and is widely used to study cerebral aging. As with humans, it displays age-related cerebral atrophy that is associated with cognitive alterations (Picq et al., 2012; Sawiak et al., 2014), age-related accumulation of amyloid and tau lesions (Kraska et al., 2011), age-related increase of iron accumulation in the pallidum and substantia nigra (Dhenain et al., 1998). This animal is now used to characterize the impact of pathological processes as prediabetes on the brain (Djelti et al., 2016), to induce Alzheimer-like pathologies (Gary et al., 2019; Lam et al., 2021) as well as to assess interventions that can modulate cerebral aging (Pifferi et al., 2018).

First, we described variations of gluCEST contrast distribution throughout the entire brain. Second, we characterized brain regions associated with age-related reduction of gluCEST contrast. Some functional regions are more intensely inter-connected between each other than to the rest of the brain, forming a level of functional organization called large-scale network. In the last part of the study, gluCEST contrast was evaluated within cerebral networks identified in mouse lemurs (Garin et al., 2021). The highest gluCEST contrast was found in the limbic network

and in high-level cortical networks such as the fronto-temporal network (FTN) and the fronto-parietal network (FPN). The FTN and FPN present homologies with human networks such as with the default mode network (DMN), the dorsal attentional network (DAN) and the executive control network (ECN) (Garin et al., 2021). Age lowered gluCEST contrast in the FTN and in the limbic network, which suggests that these two networks are prone to glutamate impairments.

2. Materials and methods

2.1. Animals and breeding

This study was carried out in accordance with the recommendations of the European Communities Council directive (2010/63/EU). The protocol was approved by the local ethics committees CEtEA-CEA DSV IdF (authorizations 201506051736524 VI (APAFIS#778)). All mouse lemurs studied were born in the laboratory breeding colony of the CNRS/MNHN in Brunoy, France (UMR 7179 CNRS/MNHN) and bred in our laboratory (Molecular Imaging Research Center, CEA, Fontenay-aux-Roses).

Thirty-three mouse lemurs (21 males and 12 females) were initially included in this study. Four animals that presented brain lesions or artefacted MR images were excluded from the analysis. Fourteen animals ranging from 1.3 to 3.8 years old (mean±SD: 2.1±0.8 years) were grouped together to form the “middle-aged lemurs cohort” (Table 1). Fifteen animals ranging from 8.0 to 10.8 years old (mean±SD: 8.8±1.1 years) were grouped together to form the “old lemurs cohort” (Table 1). Housing conditions were cages containing one or two lemurs with jumping and hiding enrichment, temperatures 24–26°C, relative humidity 55% and seasonal lighting (summer: 14 hours of light/10 hours of dark; winter: 10 hours of light/14 hours of dark). Food consisted of fresh apples and a homemade mixture of bananas, cereals, eggs and milk. Animals had free access to tap water. None of the animals had previously been involved in pharmacological trials or invasive studies.

2.2. Phantom preparation

A phantom containing 10 mM of glutamate (SigmaAldrich, USA) was prepared in phosphate buffered saline (PBS). The pH of the solution was adjusted to 7 to match physiological conditions. Serial dilutions (5/2.5/1.25/0.62/0 mM) were prepared and pH adjusted in order to measure the concentration-dependency of the gluCEST

contrast.

2.3. Animal preparation and MRI acquisition

All scanning was under isoflurane anaesthesia at 1.25-1.5% in air, with respiratory rate monitored to confirm animal stability until the end of the experiment. Body temperature was maintained by an air heating system at 32°C, inducing a natural torpor in mouse lemurs (Aujard and Vasseur, 2001). This has the advantage of allowing a low anaesthesia level without reawakening.

The MRI system was an 11.7 T Bruker BioSpec (Bruker, Ettlingen, Germany) running ParaVision 6.0.1 with a volume coil for radiofrequency transmission and a quadrature surface coil for reception (Bruker, Ettlingen, Germany).

Anatomical images were acquired using a T_2-weighted multi-slice multi-echo (MSME) sequence: repetition time (TR) = 5000 ms, echo time (TE) = 17.5 ms, field of view (FOV) = 32 × 32 mm, 75 slices of 0.2 mm thickness, 6 echoes, inter echo time (IES) = 5 ms, resolution = 200 µm isotropic, acquisition duration: 10 min.

GluCEST images covering the brain from prefrontal cortex to the occipital cortex were acquired with a 2D fast spin-echo sequence: TR = 20000 ms, TE = 6 ms, FOV = 24 × 24 mm, 12 slices of 1.5 mm thickness, resolution = 0.250 x 0.250 μm^2, acquisition duration 33 m. The MAPSHIM routine was applied in a voxel encompassing the slices of interest in order to reach a good shim on gluCEST images. gluCEST images were preceded by a frequency-selective continuous wave saturation pulse and acquired with a saturation pulse applied during T_{sat} = 1 s, composed by 10 broad pulses of 100 ms, with 20 µs inter-delay and an amplitude B_1 = 5 µT. The frequency of the saturation pulse $\Delta\omega$ was applied in a range from –5 ppm to 5 ppm with a step of 1 ppm. *In vivo*, CEST contrast can be hampered by several competing factors such as direct saturation transfer (DS) of free water and background magnetization transfer (MT). We supposed DS symmetrical with respect to water frequency and suppressed by asymmetrical analysis its contribution to CEST contrast (Sun et al., 2005; van Zijl and Yadav, 2011; Zhou and van Zijl, 2006). B_0 inhomogeneities were corrected using the Water Saturation Shift Reference (WASSR) method (Kim et al., 2009) with a saturation pulse applied around the water frequency ($\Delta\omega$ in a range from -1 ppm to 1 ppm with a step of 0.1 ppm) with an amplitude B_1 = 0.2 µT. Before gluCEST protocol, a B_1 map was acquired with the double angle method (Stollberger and Wach, 1996). Two images with long repetition

time (TR = 15000 ms) were acquired with preparation pulses flip angles of either 30° or 60°.The same normalization method, using RF pulse amplitude for a flip angle of 30° (B_{1ref}), as proposed in the literature was used to calculate relative B_1 map (B_1/B_{1ref}, unitless) (Cai et al., 2012).

2.4. MRI pre-processing

CEST images were first processed pixel-by-pixel and analyzed using in-house programs developed on MATLAB software (MathWorks Inc., Natick, MA) used to generate Z-spectra by plotting the longitudinal magnetization as a function of saturation frequency. The gluCEST contrast was isolated using Asymmetrical Magnetization Transfer Ratio (MTRasym) (Liu et al., 2010) and was calculated as follows: MTRasym(Δω) = 100 × (Msat(–Δω) – Msat(+Δω)) / Msat(–5 ppm), Msat(±Δω) being the magnetization acquired with saturation pulse applied at '+' or '–' Δω ppm. GluCEST images were calculated with Δω centered at ± 3 ppm. GluCEST image was converted into NIfTI-1 format.

Anatomical images were exported as DICOM files then converted into NIfTI-1 format. Then spatial pre-processing was performed using the python module sammba-mri (SmAll MaMmals BrAin MRI; http://sammba-mri.github.io) (Celestine et al., 2020) which, using nipype for pipelining (Gorgolewski et al., 2011), leverages AFNI (Cox, 1996) for most steps and RATS (Oguz et al., 2014) for brain extraction. Anatomical images were mutually registered to create a study template, which was further registered to a high-resolution anatomical mouse lemur template of the functional atlas (Garin et al., 2021). Then, gluCEST images were brought into the same space of the mouse lemur template by applying transformation from individual anatomical space to the study template.

2.5. GluCEST contrast extraction and statistical analysis

To calculate regional distribution of gluCEST contrast and its differences between groups, we extracted gluCEST contrast using a mouse lemur digital atlas (https://www.nitrc.org/projects/mouselemuratlas; (Nadkarni et al., 2019), large scale network maps (http://www.nitrc.org/projects/prim_func_2020/; (Garin et al., 2021) as well as the function NiftiLabelsMasker from Nilearn (Abraham et al., 2014).

Inter-individual differences between middle-aged and old groups were first evaluated using voxel wise statistical analysis (AFNI 3dttest++ (Cox, 1996)). Voxel wise analysis was performed only in regions with high gluCEST contrast (ten percent

of the highest gluCEST voxels were kept). Cluster size (40 voxels) was estimated using AFNI (-Clusterize) with $p<0.03$ (uncorrected)). Using map_threshold from Nilearn (Abraham et al., 2014), we extracted from the Ttest map clusters of voxels superior to 40 associated to $p<0.03$.

Then, we evaluated differences of gluCEST contrast between middle-aged and old groups at different levels of segmentation (anatomy/network). Statistical differences between middle-aged and old animals were estimated using Kruskal-Wallis H-test. These complementary analyses were performed to test the reproducibility of the voxel wise results as well as to evaluate the fit between anatomy/network and dysfunction.

2.6. Data availability

The template and atlas used in this study are available for download in NIfTI-1 format at https://www.nitrc.org/projects/mouselemuratlas. The code developed to create and manipulate the template has been refined into general procedures for registering small mammal brain MR images, available within a python module sammba-mri (SmAll-maMMals BrAin MRI; https://sammba-mri.github.io). MR images used in this study can be made available upon request after signing a data sharing agreement required by authors' institution.

3. Results

3.1. Phantom study

The GluCEST effect is linearly proportional to the glutamate concentration in the 1 to 10 mM (Suppl. Fig. 1). The detection threshold in vitro with our configuration is estimated around 0.5 to 1 mM. This "dose-response" of gluCEST contrast in function of glutamate concentration is consistent with previous reports in the literature (Cai et al., 2012).

3.2. GluCEST contrast distribution in middle-aged adult mouse lemurs

GluCEST images were acquired from 29 anaesthetised mouse lemurs (isoflurane 1.25-1.5%) at 11.7 Tesla (Table 1). The mean ratio B_1/B_{1ref} (0.98 ± 0.02, Fig. 1A) and B_0 shift (0.03 ± 0.14 ppm, Fig. 1B) measured into imaging slices showed homogeneity of B_1 and B_0 fields through the brain. An example of average Zspectrum and asymmetrical magnetization transfer ratio (MTRasym in %) calculated in the area

21 (temporal cortex) of the two groups is shown in Fig. 1D.

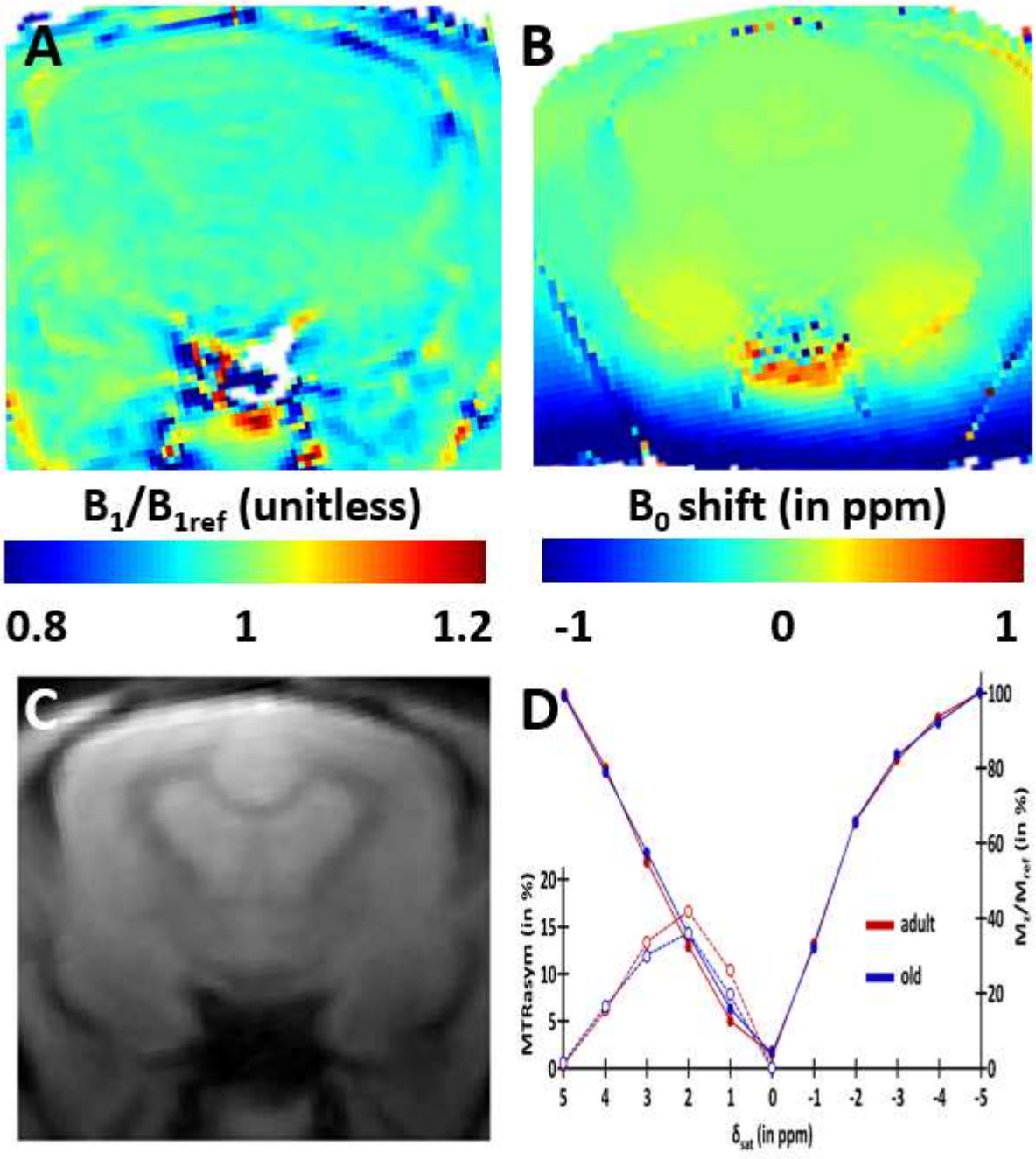

Figure 1. B_1, B_0 and regional Zspectrum and MTRasym (in %) in area 21 (temporal region) of middle-aged adult and old mouse lemurs.
(A) B_1, (B) B_0 maps and (C) anatomical image acquired in one representative mouse lemur. B_0 was calculated before WASSR correction. (D) average Zspectrum and MTRasym in area 21 (temporal region) of middle-aged adult (red) and old (blue) mouse lemurs (mean ± SEM).

Then, GluCEST contrast was analysed in middle-aged adults (n=14, 1.3 to 3.8 year-old, mean±SD: 2.1±0.8 years, Table 1). Regions with the highest gluCEST contrast (MTRasym at 3 ppm) were found in subcortical regions and cortical regions (Fig. 2A, Fig. 3A). Subcortical regions with the highest contrast (median>16) were the

nucleus accumbens, septum, basal forebrain, putamen, claustrum and caudate nucleus. Cortical regions with the highest contrast were frontal regions from the anterior cingulate areas (area 25 (subgenual area) and 24 (anterior cingulate cortex)) and area 4 (primary motor cortex). Cortical distribution of gluCEST contrast is further displayed on 3D views of the brain in Fig. 2B. This figure reflects an average surface map of MTRasym, normalized by the average signal of the brain. This normalization allows visualizing variation strictly based on the distribution of gluCEST contrast and not to inter-individual variations.

GluCEST contrast was especially low in the entorhinal cortex (area 28), retrosplenial region (area 30), occipital cortex (area 17), thalamus and the colliculi.

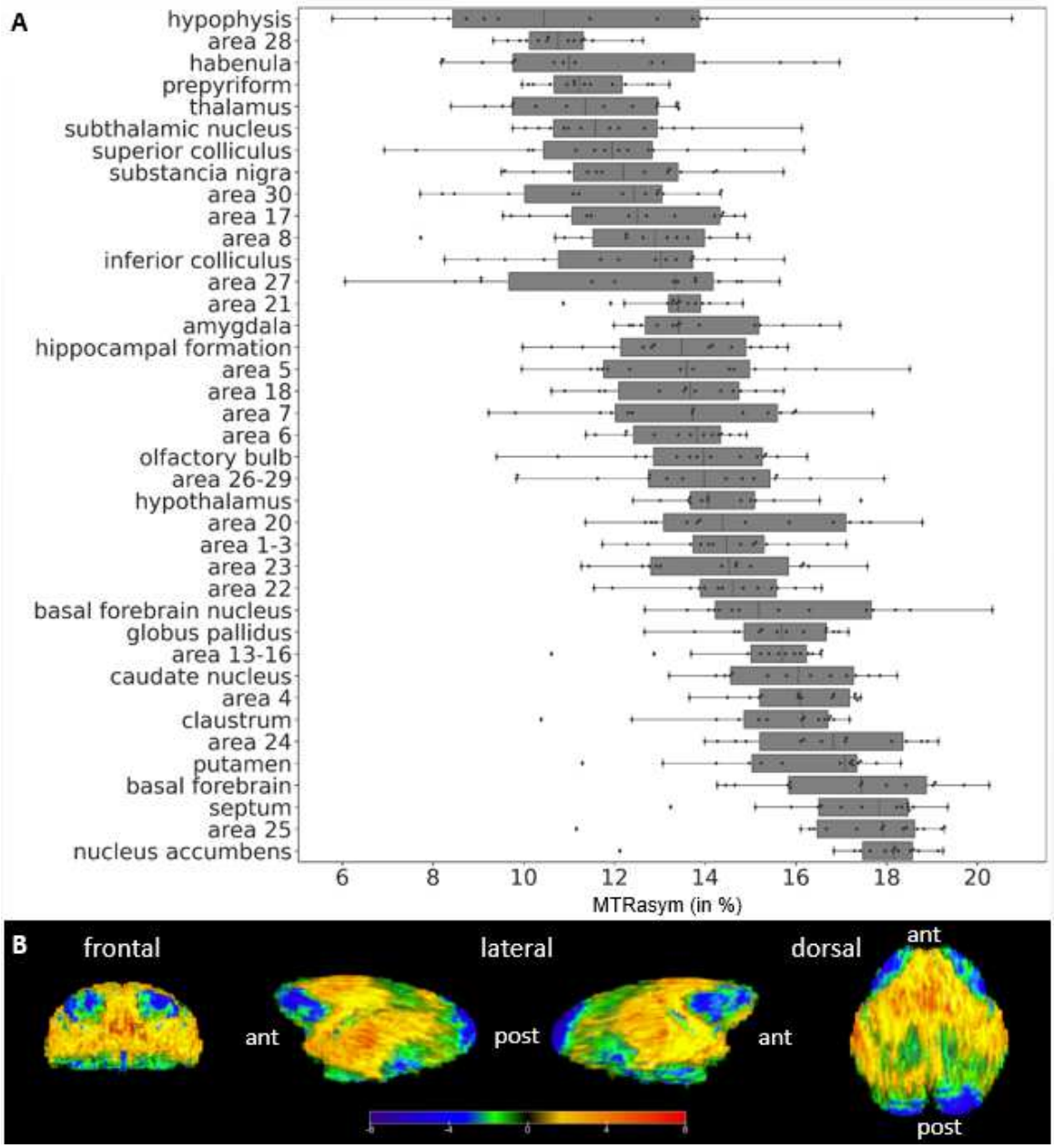

Figure 2. Regional MTRasym (in %) of middle-aged adult mouse lemurs.

(A) MTRasym in different brain regions of middle-aged adult mouse lemurs (n=14) ranked based on their group median value. Elevated MTRasym is observed within regions encompassing the nucleus accumbens, septum, basal forebrain, putamen, and anterior cingulate regions (areas 24 and 25). (B) 3D surface map of the gluCEST contrast showing regional signal variations. Color map: average surface map of MTRasym, normalized by the average signal of the brain. ant: anterior part of the brain, post: posterior part of the brain.

3.3. Age-related regional alterations of GluCEST contrast

3.3.1. Voxel based analysis

Inter-individual differences between maps of MTRasym in middle-aged (Fig. 3A) and old groups (Fig. 3B) were evaluated using voxel wise statistical analysis (Fig. 3D). This analysis highlighted a significant statistical decrease in voxels belonging to the globus pallidus, nucleus accumbens, and to a lower extent hypothalamus and septum. Within the cortex, signal was reduced in area 4 (primary motor cortex) and area 6 (premotor cortex and supplementary motor area) (Nadkarni et al., 2019) (Fig. 3D).

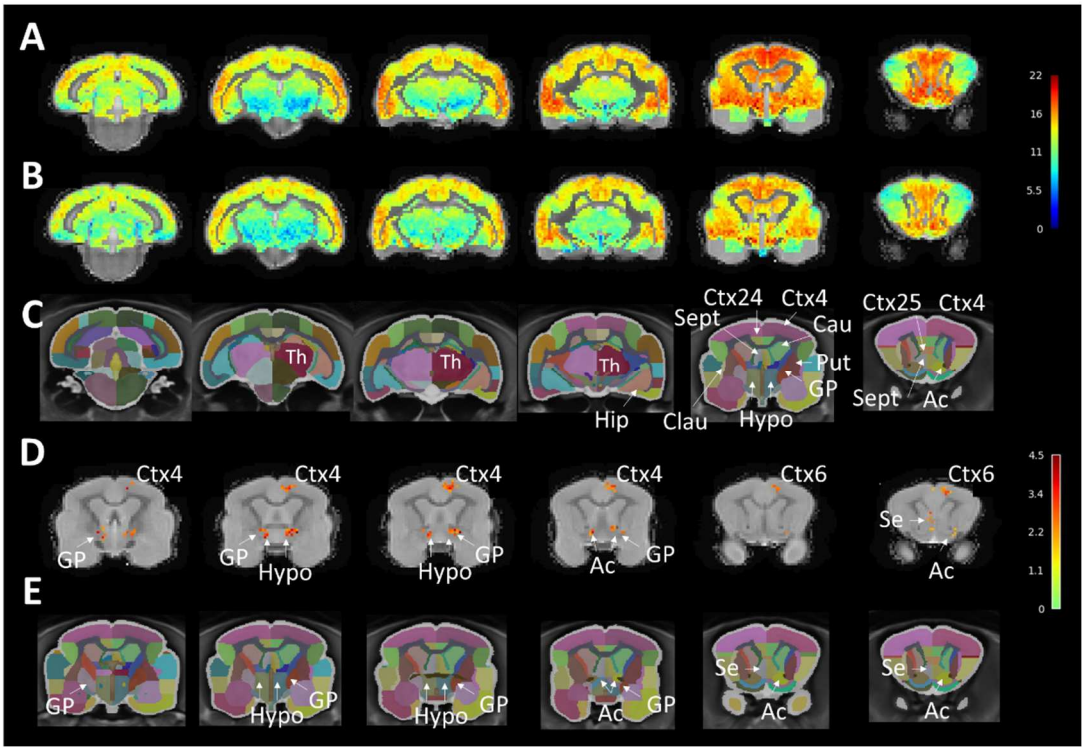

Figure 3. gluCEST contrast (MTRasym) **in middle-aged and old mouse lemurs.** Average MTRasym in middle-aged (A) and old mouse lemurs (B). Anatomical view of the mouse lemur brain corresponding to the displayed sections are displayed in C (Nadkarni et al., 2019). Significant statistical decrease of the gluCEST contrast was detected using voxelwise analysis in the globus pallidus, nucleus accumbens, and to a lower extent hypothalamus and septum (D). Within the cortex, signal was

reduced in area 4 (primary motor cortex) and area 6 (premotor cortex and supplementary motor area). The slices posterior and anterior to those shown in figure D and E did not display any significant differences. E displayed an anatomical view of the mouse lemur sections shown in D (Nadkarni et al., 2019). Ac: Nucleus accumbens; Se: Septum; bf: Basal forebrain; Cau: Caudate nucleus; Clau: Claustrum; GP: Globus pallidus; Hip: Hippocampus; Hypo: Hypothalamus; Sept: Septum; Th: Thalamus. Scale bars in A-C: gluCEST contrast, in D: t-value.

3.3.2. Atlas based analysis

Comparison of gluCEST contrast n middle-aged and old animals was also performed using an atlas-based approach. This analysis confirmed that aging is associated with a decrease of gluCEST contrast in the globus pallidus (*p = 0.00025*, Kruskal-Wallis H-test), nucleus accumbens (*p = 0.0013*, Kruskal-Wallis H-test). It detected additional subcortical regions with an age-related gluCEST contrast decrease in the hypophysis (*p = 0.0052*, Kruskal-Wallis H-test), septum (*p = 0.016*, Kruskal-Wallis H-test), and basal forebrain (*p = 0.032*, Kruskal-Wallis H-test). The hypothalamus that displayed focal reduction of gluCEST contrast was not detected by this atlas-based approach. The cortical area 6 was detected with an atlas-based approach (*p = 0.029*, Kruskal-Wallis H-test) as well as additional cortical regions (*e.g.* area 25 (*p = 0.026*, Kruskal-Wallis H-test) and area 21 (middle temporal area, *p = 0.0040*, Kruskal-Wallis H-test)) (Fig. 4).

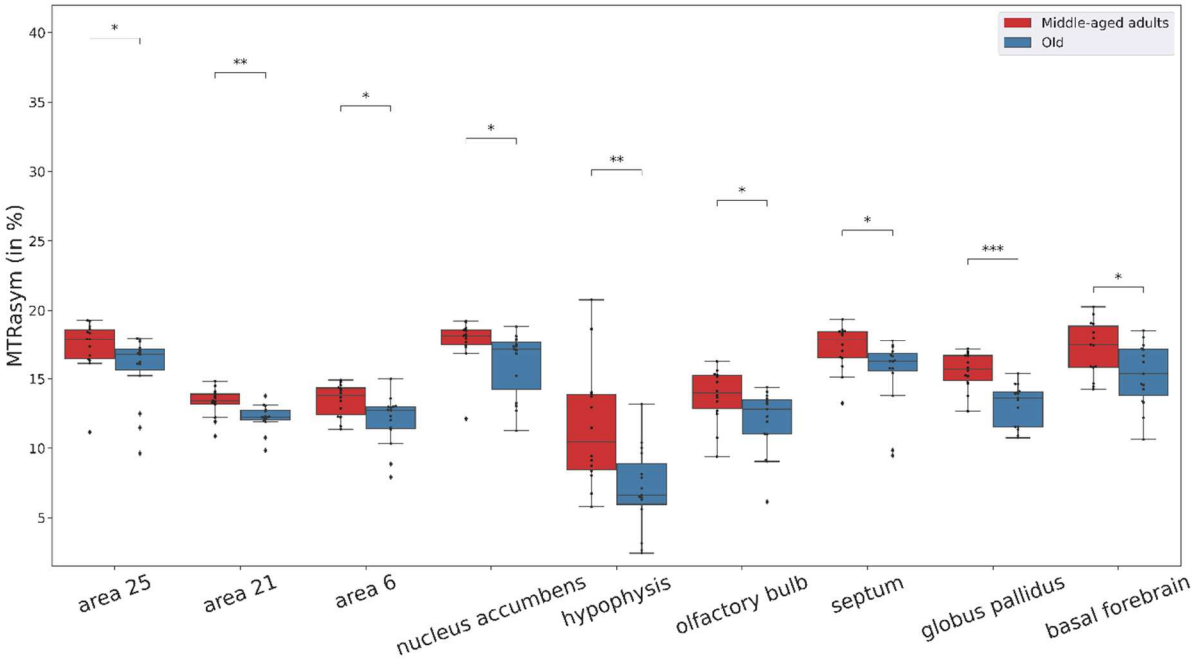

Figure 4. Significant differences of gluCEST contrast between middle-aged and old mouse lemurs as detected with an atlas-based approach.
*: p <0.05; **: p <0.01, ***: p < 0.001, ****: p < 0.0001.

3.3.3. Age-related impairments of gluCEST contrast involves large scale networks

We then evaluated the extracted contrast within cerebral networks previously reported in mouse lemurs (Garin et al., 2021). GluCEST differences between middle-aged and old animals were found in the fronto-temporal network (Fig. 5; *p = 0.016*, Kruskal-Wallis H-test) and the evaluative limbic network (*p = 0.026*, Kruskal-Wallis H-test). The fronto-temporal network involved the frontal anterior medial and lateral regions, the precentral cortex, all the temporal regions, the parietal posterior cortex, the anterior and medial cingulum cortices, and the insular cortex. The evaluative-limbic network included limbic structures, the insula, as well as subcortical structures.

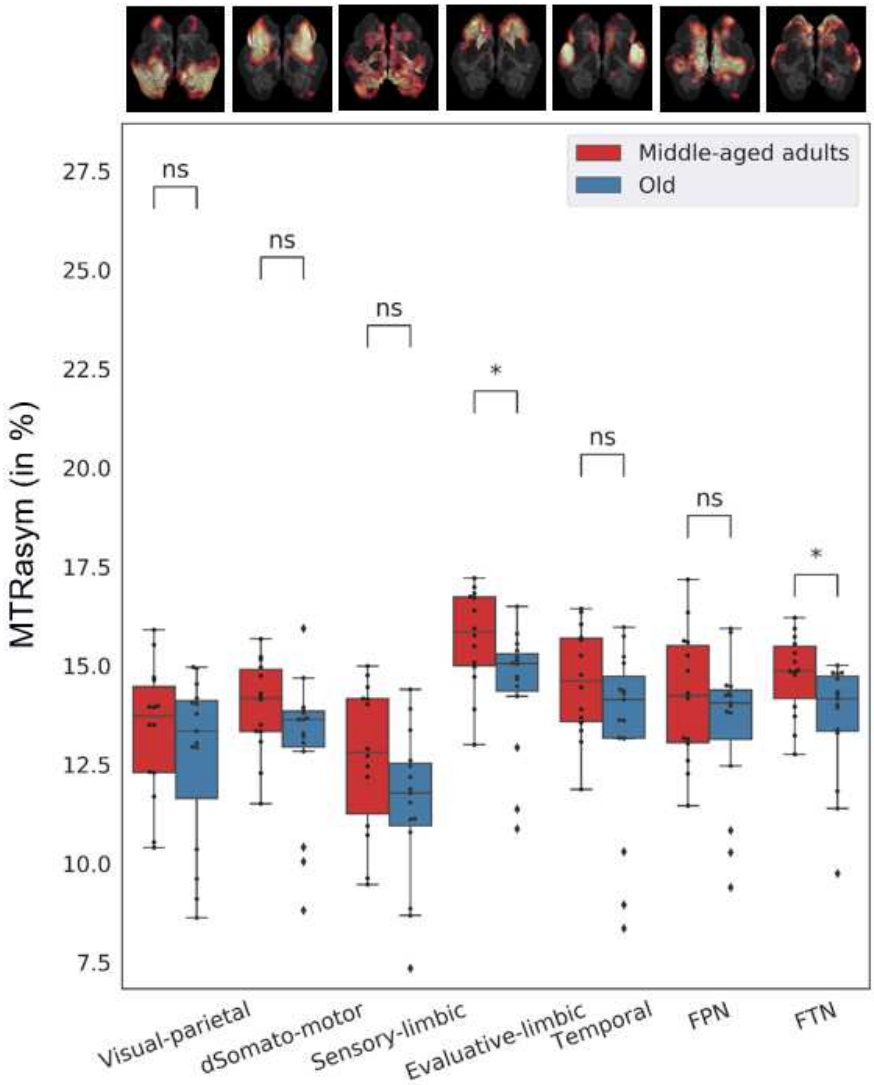

Figure 5. gluCEST contrast within large-scale networks of middle-aged and old mouse lemurs.
Contrast was lower in the evaluative limbic network (*p = 0.026*, Kruskal-Wallis H-

test) and in the fronto-temporal network (FTN, *p = 0.016*, Kruskal-Wallis H-test) of old animals when compared to middle-aged animals. At the top of the figure, large-scale networks are illustrated using images based on Garin et al. (Garin et al., 2021). *: p < 0.05; **: p < 0.01, ***: p < 0.001, ****: p < 0.0001. FPN: Fronto-parietal network.

4. Discussion

This study characterized for the first-time gluCEST contrast distribution and its age-related changes throughout the entire brain of a non-human primate. High field is a key condition to produce gluCEST images with a meaningful signal to noise ratio. Given its small body size, the mouse lemur could fit in small-bore high field MRI scanner, which opened the possibility for gluCEST imaging in a non-human primate.

4.1. Distribution of gluCEST contrast in normal middle-aged animals

Glutamate is an essential amino acid and has the highest amino acid concentration of the brain. It is involved in several metabolic pathways related to energy metabolism and oxidative stress (Sonnewald, 2014; Zhou and Danbolt, 2014). It is also the major excitatory neurotransmitter in the central nervous system (Cooper and Jeitner, 2016).

The main glutamate pathways involve projections **i.** from the prefrontal cortex to the striatum (caudate nucleus and putamen: cortico-striatal pathway) and the nucleus accumbens (cortico-accumbens pathway), **ii.** from the prefrontal cortex to brain-stem nuclei (cortico-brainstem pathway), **iii.** from the prefrontal cortex to the thalamus (cortico-thalamic pathway). **iv.** from the thalamus to the cortex (thalamo-cortical pathway), and **v.** from the cortex to the cortex (cortico-cortical pathways) (Greenamyre, 2001; Schwartz et al., 2012).

We found high gluCEST contrast in several regions involved in these pathways. In cortical regions, high gluCEST contrast was observed in the anterior cingulate regions (Brodmann area 25 (subgenual area) and 24 (anterior cingulate cortex)) and premotor cortex (area 6). These regions fit with human “cortico-striatal/accumbens/thalamic/brain stem” glutamate pathways. Most of the subcortical regions in which we detected high gluCEST contrast were also involved in these pathways. Indeed, high levels were found in the putamen and caudate nucleus, involved in the cortico-striatal pathway. Numerous studies outlined the strong cortical glutamatergic projections on these structures (Galvan et al., 2006; Lanciego et al.,

2012). The nucleus accumbens involved in the cortico-striatal pathway also had high gluCEST contrast. However, some other regions which are less involved in these pathways such as the septum and basal forebrain, also had high gluCEST contrasts. Of note, neurotransmission is governed by few micromolars of extracellular glutamate so one can hypothesize that the pool of glutamate neurotransmitter contributes very slightly to the gluCEST contrast. Thus, even if gluCEST changes occur close to glutamate pathways, they do not directly reflect changes of neurotransmitters, but mainly pools of glutamate involved in metabolic pathways.

4.2. Age-related changes of gluCEST contrast

In the second part of our study, we showed that aging leads to reduction of gluCEST contrast in subcortical regions such as the nucleus accumbens, septum, basal forebrain, globus pallidus, hypophysis and to a lower extent hypothalamus. In the mouse lemur cortex, the reduction of gluCEST contrast occurred in frontal regions (anterior cingulate regions (areas 24-25), area 6), temporal regions (area 21). Parietal regions (area 4) also displayed some age-related changes. Minor differences between voxel-based and atlas-based analyses were observed. They can easily be explained by **i.** the exclusion of low gluCEST contrast areas in voxel-based analysis **ii.** the divergence of resolution (voxel vs anatomical region) **iii.** Atlas-based analysis results are displayed without correction for multiple comparisons. The few differences between the two analyses do not modify the interpretation of our study but their similarities strengthen the robustness of the detected alterations. In humans, an age-related glutamate reduction has been found in similar regions as in mouse lemurs. In particular, a reduction of glutamate levels was highlighted in the globus pallidus and the putamen using MR spectroscopy based on voxels that embedded these regions. Lower glutamate levels in these regions were associated with cognitive decline (Zahr et al., 2008). An age-related reduction of glutamate levels was also reported in the motor cortex of humans (Kaiser et al., 2005).

In the last part of the study, we showed that age-related changes of gluCEST contrast involved two large-scale networks: the fronto-temporal network and the evaluative limbic network. The fronto-temporal network is partly homologous to the human executive control network, DMN, salience and fronto-temporal networks (Garin et al., 2021). It was suggested that this network is involved in interoception and in self-referential decisions (Garin et al., 2021). We can speculate that age-

related changes of glutamate levels in this network may impair these functions, although it is difficult to test them in lemurs. The evaluative limbic network subserves behavioural responses to the positive/negative valence of stimuli as well as to the internal state of the body (Garin et al., 2021). In humans, several reports highlighted age-related impairments of large-scale networks (Ferreira and Busatto, 2013; Zhang et al., 2014). Impairments of white matter and dopamine as well as accumulation of amyloid in the brain have been suggested as potential culprits for these changes (Ferreira and Busatto, 2013). Our study suggests, that for at least some networks, glutamate level changes can also be involved in network impairments, although the impact of glutamate changes on network function will have to be further investigated in the future.

4.3. Interpretation of gluCEST contrast changes

This study evaluated gluCEST contrast changes in different brain regions of the mouse lemurs and their evolution with aging. Theoretical as well as experimental studies have shown that approximately 70% of gluCEST value is due to glutamate (Bagga et al., 2018; Cai et al., 2012). Here, as in several other studies, we analyzed phantoms containing glutamate (with levels similar to those expected to be present in the brain: about 8 mM) and found that gluCEST contrast follows a linear dependency with glutamate concentration in the 1 to 10 mM range with the same sequence and same saturation parameters used for *in vivo* imaging. In previous in vivo studies, changes seen on gluCEST images where shown to be consistent with changes of glutamate levels observed with proton magnetic resonance spectroscopy (Cai et al., 2012; Flament et al., 2015). However, one potential confounding factor in interpreting GluCEST results is the signal contribution from protein lysine amine protons (Cui et al., 2020). Thus, a significant amount of cerebral proteins containing lysine residues can also contribute to changes in gluCEST contrast. In addition, gluCEST indirectly detects solute molecules by observing water signal changes and thus depends on multiple nonspecific tissue parameters, including the water longitudinal (T1), transverse (T2) relaxation times, and the semisolid magnetization transfer effect (Cui et al., 2020). These changes can modulate regional differences in gluCEST contrast, including age-related changes. Therefore, gluCEST contrast should be regarded as a proxy for glutamate without ruling out any non-glutamate-related explanation for its changes. In particular the impact of changes of cerebral protein levels in different

brain regions or during aging should not be neglected. T1, T2 and semisolid magnetization transfer effect are expected to be lower, even if they can not be totally neglected. The T2 effect was largely cancelled out by the normalization of the gluCEST image. We can not totally rule out a small T1 effect, although to the best of our knowledge age-related variations of this parameter are not reported in mouse lemurs or rats. In humans, a small age-related T1 increase was reported (Hagiwara et al, 2021). This would induce a slight increase of gluCEST contrast and we found an age-related decrease of gluCEST contrast. Finally, with our saturation protocol (strong B1, Tsat = 1s), the sensitivity of our gluCEST sequence toward semisolid magnetization transfer is limited.

5. Conclusion

This study characterized gluCEST contrast at the whole brain level in a primate and reported age-related cerebral alterations in several key regions. This technic appears to be an essential tool to better understand the various mechanisms altering the brain and promises multiple applications for the diagnosis, follow up, treatment efficiency of neurodegenerative diseases.

6. Acknowledgements

We thank the France-Alzheimer Association, Plan Alzheimer Foundation and the French Public Investment Bank's "ROMANE" program for funding this study. The 11.7T MRI scanner was funded by a grant from NeurATRIS: A Translational Research Infrastructure for Biotherapies in Neurosciences ("Investissements d'Avenir", ANR-11-INBS-0011). C.G. was financed by the French Ministère de l'Enseignement Supérieur, de la Recherche et de l'Innovation.

7. Competing interests

The authors do not have financial and non-financial competing interests in relation to the work described.

8. Author contributions

C.M.G., J.F., and M.D. contributed to the study conception and design. J.P. and J.F. designed the gluCEST sequences, C.M.G. and N.A.N. designed registrations strategies and pipelines. C.M.G., J.F., and M.D. wrote the manuscript. All authors

commented on previous versions of the manuscript. All authors read and approved the final manuscript.

9. References

Abraham, A., Pedregosa, F., Eickenberg, M., Gervais, P., Mueller, A., Kossaifi, J., Gramfort, A., Thirion, B., Varoquaux, G., 2014. Machine learning for neuroimaging with scikit-learn. Front. Neuroinform. 8(14) DOI: 10.3389/fninf.2014.00014.

Hagiwara, A., Fujimoto, K., Kamagata, K., Murata, S., Irie, R., Kaga, H., Someya, Y., Andica, C., Fujita, S., Kato, S., Fukunaga, I., Wada, A., Hori, M., Tamura, Y., Kawamori, R., Watada, H., Aoki, S., 2021. Age-related changes in relaxation times, proton density, myelin, and tissue volumes in adult brain analyzed by 2-dimensional quantitative synthetic magnetic resonance imaging. Invest. Radiol. 56(3), 163-72. DOI: 10.1097/Rli.0000000000000720.

Aujard, F., Vasseur, F., 2001. Effect of ambient temperature on the body temperature rhythm of male gray mouse lemurs (*Microcebus murinus*). Int. J. Primatol. 22(1), 43-56. DOI: 10.1023/A:1026461914534.

Bagga, P., Pickup, S., Crescenzi, R., Martinez, D., Borthakur, A., D'Aquilla, K., Singh, A., Verma, G., Detre, J.A., Greenberg, J., Hariharan, H., Reddy, R., 2018. In vivo GluCEST MRI: Reproducibility, background contribution and source of glutamate changes in the MPTP model of Parkinson's disease. Sci Rep-Uk 8, Artn 2883. DOI: 10.1038/S41598-018-21035-3.

Cai, K., Haris, M., Singh, A., Kogan, F., Greenberg, J.H., Hariharan, H., Detre, J.A., Reddy, R., 2012. Magnetic resonance imaging of glutamate. Nat. Med. 18(2), 302-306. DOI: 10.1038/nm.2615.

Carrillo-de Sauvage, M.A., Flament, J., Bramoulle, Y., Ben Haim, L., Guillermier, M., Berniard, A., Auregan, G., Houitte, D., Brouillet, E., Bonvento, G., Hantraye, P.,

Valette, J., Escartin, C., 2015. The neuroprotective agent CNTF decreases neuronal metabolites in the rat striatum: an in vivo multimodal magnetic resonance imaging study. J. Cerebr. Blood F. Met. 35(6), 917-921. DOI: 10.1038/jcbfm.2015.48.

Celestine, M., Nadkarni, N.A., Garin, C., Bougacha, S., Dhenain, M., 2020. Sammba-MRI, a library for small animal neuroimaging data processing in Python. Front. Neuroinform. 14:24. DOI: 10.3389/fninf.2020.00024.

Cooper, A.J.L., Jeitner, T.M., 2016. Central role of glutamate metabolism in the maintenance of nitrogen homeostasis in normal and hyperammonemic brain. Biomolecules 6(2), Artn 16. DOI: 10.3390/Biom6020016.

Cox, R.W., 1996. AFNI: software for analysis and visualization of functional magnetic resonance neuroimages. Comput. Biomed. Res. 29(3), 162-173. DOI: 10.1006/cbmr.1996.0014.

Cui, J., Zhang, X.-Y., Xie, J., Gochberg, D.F., Zu, Z.L. 2020. Towards the molecular origin of glutamate CEST (GluCEST) imaging in rat brain. Magn. Reson. Med. 83(4), 1405-17. DOI: 10.1002/mrm.28021.

Dhenain, M., Duyckaerts, C., Michot, J.-L., Volk, A., Picq, J.-L., Boller, F., 1998. Cerebral T2-weighted signal decrease during aging in the mouse lemur primate reflects iron accumulation. Neurobiol. Aging 19(1), 65-69.

Djelti, F., Dhenain, M., Terrien, J., Picq, J.L., Hardy, I., Champeval, D., Perret, M., Schenker, E., Epelbaum, J., Aujard, F., 2016. Impaired fasting blood glucose is associated to cognitive impairment and cerebral atrophy in middle-aged non-human primates. Aging (Albany NY) 9(1), 173-186. DOI: 10.18632/aging.101148.

Ferreira, L.K., Busatto, G.F., 2013. Resting-state functional connectivity in normal brain aging. Neurosci. Biobehav. Rev. 37(3), 384-400. DOI: 10.1016/j.neubiorev.2013.01.017.

Flament, J., Gary, C., Koch, J., Pifferi, F., Comoy, E., Picq, J.-L., Valette, J., Dhenain, M.,2015. GluCEST imaging in a primate model of Alzheimer's disease. 23rd Annual Meeting of the International Society for Magnetic Resonance in Medicine.

Galvan, A., Kuwajima, M., Smith, Y., 2006. Glutamate and GABA receptors and transporters in the basal ganglia: What does their subsynaptic localization reveal about their function? Neuroscience 143(2), 351-375. DOI: 10.1016/j.neuroscience.2006.09.019.

Garin, C.M., Nadkarni, N.A., Landeau, B., Chételat, G., Picq, J.-L., Bougacha, S., Dhenain, M., 2021. Resting state functional atlas and cerebral networks in mouse lemur primates at 11.7 Tesla. NeuroImage 226, 117589. DOI: 10.1016/j.neuroimage.2020.117589.

Gary, C., Lam, S., Herard, A.S., Koch, J.E., Petit, F., Gipchtein, P., Sawiak, S.J., Caillierez, R., Eddarkaoui, S., Colin, M., Aujard, F., Deslys, J.P., French Neuropathology Network, Brouillet, E., Buée, L., Comoy, E.E., Pifferi, F., Picq, J.-L., Dhenain, M., 2019. Encephalopathy induced by Alzheimer brain inoculation in a non-human primate. Acta Neuropathol. Commun. 7(126) DOI: 10.1186/s40478-019-0771-x.

Gorgolewski, K., Burns, C.D., Madison, C., Clark, D., Halchenko, Y.O., Waskom, M.L., Ghosh, S.S., 2011. Nipype: a flexible, lightweight and extensible neuroimaging data processing framework in python. Front. Neuroinform. 5(13) DOI: 10.3389/fninf.2011.00013.

Greenamyre, J.T., 1986. The role of glutamate in neurotransmission and in neurologic disease. Arch. Neurol. 43(10), 1058-1063. DOI: 10.1001/archneur.1986.00520100062016.

Greenamyre, J.T., 2001. Glutamatergic influences on the basal ganglia. Clin

Neuropharmacol 24(2), 65-70. DOI: 10.1097/00002826-200103000-00001.

Haris, M., Nath, K., Cai, K.J., Singh, A., Crescenzi, R., Kogan, F., Verma, G., Reddy, S., Hariharan, H., Melhem, E.R., Reddy, R., 2013. Imaging of glutamate neurotransmitter alterations in Alzheimer's disease. NMR Biomed. 26(4), 386-391. DOI: 10.1002/nbm.2875.

Kaiser, L.G., Schuff, N., Cashdollar, N., Weiner, M.W., 2005. Age-related glutamate and glutamine concentration changes in normal human brain: H-1 MR spectroscopy study at 4T. Neurobiol. Aging 26(5), 665-672. DOI: 10.1016/j.neurobiolaging.2004.07.001.

Kim, M., Gillen, J., Landman, B.A., Zhou, J.Y., van Zijl, P.C.M., 2009. Water saturation shift referencing (WASSR) for chemical exchange saturation transfer (CEST) experiments. Magn. Reson. Med. 61(6), 1441-1450. DOI: 10.1002/mrm.21873.

Kirvell, S.L., Esiri, M., Francis, P.T., 2006. Down-regulation of vesicular glutamate transporters precedes cell loss and pathology in Alzheimer's disease. J. Neurochem. 98(3), 939-950. DOI: 10.1111/j.1471-4159.2006.03935.x.

Kraska, A., Dorieux, O., Picq, J.-L., Petit, F., Bourrin, E., Chenu, E., Volk, A., Perret, M., Hantraye, P., Mestre-Frances, N., Aujard, F., Dhenain, M., 2011. Age associated cerebral atrophy in mouse lemur Primates. Neurobiol. Aging 32(5), 894–906. DOI: 10.1016/j.neurobiolaging.2009.05.018.

Lam, S., Petit, F., Hérard, A.-S., Boluda, S., Eddarkaoui, S., Guillermier, M., The Brainbank Neuro-CEB Neuropathology Network, Buée, L., Duyckaerts, C., Haïk, S., Picq, J.-L., Dhenain, M., 2021. Transmission of amyloid-beta and tau pathologies is associated with cognitive impairments in a primate. Acta Neuropathol. Commun. 9, 165. DOI: 10.1186/s40478-021-01266-8.

Lanciego, J.L., Luquin, N., Obeso, J.A., 2012. Functional neuroanatomy of the basal ganglia. Cold Spring Harbor perspectives in medicine 2(12), ARTN a009621. DOI: 10.1101/cshperspect.a009621.

Liu, G.S., Gilad, A.A., Bulte, J.W.M., van Zijl, P.C.M., McMahon, M.T., 2010. High-throughput screening of chemical exchange saturation transfer MR contrast agents. Contr. Med. Mol. Im. 5(3), 162-170. DOI: 10.1002/cmmi.383.

Nadkarni, N.A., Bougacha, S., Garin, C., Dhenain, M., Picq, J.L., 2019. A 3D population-based brain atlas of the mouse lemur primate with examples of applications in aging studies and comparative anatomy. Neuroimage 185, 85-95. DOI: 10.1016/j.neuroimage.2018.10.010.

Nanga, R.P.R., DeBrosse, C., Kumar, D., Roalf, D., McGeehan, B., D'Aquilla, K., Borthakur, A., Hariharan, H., Reddy, D., Elliott, M., Detre, J.A., Epperson, C.N., Reddy, R., 2018. Reproducibility of 2D GluCEST in healthy human volunteers at 7 T. Magn. Reson. Med. 80(5), 2033-2039. DOI: 10.1002/mrm.27362.

Niciu, M.J., Kelmendi, B., Sanacora, G., 2012. Overview of glutamatergic neurotransmission in the nervous system. Pharmacol. Biochem. Behav. 100(4), 656-664. DOI: 10.1016/j.pbb.2011.08.008.

Oguz, I., Zhang, H., Rumple, A., Sonka, M., 2014. RATS: Rapid Automatic Tissue Segmentation in rodent brain MRI. J. Neurosci. Methods 221, 175-182. DOI: 10.1016/j.jneumeth.2013.09.021.

Pepin, J., Francelle, L., Carrillo-de Sauvage, M.A., de Longprez, L., Gipchtein, P., Cambon, K., Valette, J., Brouillet, E., Flament, J., 2016. In vivo imaging of brain glutamate defects in a knock-in mouse model of Huntington's disease. Neuroimage 139, 53-64. DOI: 10.1016/j.neuroimage.2016.06.023.

Picq, J.L., Aujard, F., Volk, A., Dhenain, M., 2012. Age-related cerebral atrophy in

nonhuman primates predicts cognitive impairments. Neurobiol. Aging 33(6), 1096–1109. DOI: https://doi.org/10.1016/j.neurobiolaging.2010.09.009.

Pifferi, F., Terrien, J., Marchal, J., Dal-Pan, A., Djelti, F., Hardy, I., Chahory, S., Cordonnier, N., Desquilbet, L., Hurion, M., Zahariev, A., Chery, I., Zizzari, P., Perret, M., Epelbaum, J., Blanc, S., Picq, J.-L., Dhenain, M., Aujard, F., 2018. Caloric restriction increases lifespan but affects brain integrity in grey mouse lemur primates. Comm. Biol. 1(1), 30. DOI: 10.1038/s42003-018-0024-8.

Roalf, D.R., Nanga, R.P.R., Rupert, P.E., Hariharan, H., Quarmley, M., Calkins, M.E., Dress, E., Prabhakaran, K., Elliott, M.A., Moberg, P.J., Gur, R.C., Gur, R.E., Reddy, R., Turetsky, B.I., 2017. Glutamate imaging (GluCEST) reveals lower brain GluCEST contrast in patients on the psychosis spectrum. Mol. Psychiatry 22(9), 1298-1305. DOI: 10.1038/mp.2016.258.

Roalf, D.R., Sydnor, V.J., Woods, M., Wolk, D.A., Scott, J.C., Reddy, R., Moberg, P.J., 2020. A quantitative meta-analysis of brain glutamate metabolites in aging. Neurobiol. Aging 95, 240-249. DOI: 10.1016/j.neurobiolaging.2020.07.015.

Sailasuta, N., Ernst, T., Chang, L., 2008. Regional variations and the effects of age and gender on glutamate concentrations in the human brain. Magn. Reson. Imaging 26(5), 667-675. DOI: 10.1016/j.mri.2007.06.007.

Sawiak, S.J., Picq, J.L., Dhenain, M., 2014. Voxel-based morphometry analyses of in vivo MRI in the aging mouse lemur primate. Front. Aging Neurosci. 6, 82. DOI: 10.3389/fnagi.2014.00082.

Schwartz, T.L., Sachdeva, S., Stahl, S.M., 2012. Glutamate neurocircuitry: theoretical underpinnings in schizophrenia. Front. Pharmacol. 3, Artn 195. DOI: 10.3389/Fphar.2012.00195.

Sonnewald, U., 2014. Glutamate synthesis has to be matched by its degradation -

where do all the carbons go? J. Neurochem. 131(4), 399-406. DOI: 10.1111/jnc.12812.

Stollberger, R., Wach, P., 1996. Imaging of the active B-1 field in vivo. Magn. Reson. Med. 35(2), 246-251. DOI: DOI 10.1002/mrm.1910350217.

Sun, P.Z., van Zijl, P.C.M., Zhou, J.Y., 2005. Optimization of the irradiation power in chemical exchange dependent saturation transfer experiments. J. Magn. Reson. 175(2), 193-200. DOI: 10.1016/j.jmr.2005.04.005.

van Zijl, P.C.M., Yadav, N.N., 2011. Chemical Exchange Saturation Transfer (CEST): What is in a name and what isn't? Magn. Reson. Med. 65(4), 927-948. DOI: 10.1002/mrm.22761.

Zahr, N.M., Mayer, D., Pfefferbaum, A., Sullivan, E.V., 2008. Low striatal glutamate levels underlie cognitive decline in the elderly: Evidence from in vivo molecular spectroscopy. Cereb. Cortex 18(10), 2241-2250. DOI: 10.1093/cercor/bhm250.

Zhang, H.Y., Chen, W.X., Jiao, Y., Xu, Y., Zhang, X.R., Wu, J.T., 2014. Selective vulnerability related to aging in large-scale resting brain networks. PLoS ONE 9(10), ARTN e108807. DOI: 10.1371/journal.pone.0108807.

Zhou, J.Y., van Zijl, P.C.M., 2006. Chemical exchange saturation transfer imaging and spectroscopy. Prog. Nucl. Mag. Res. Spectro. 48(2-3), 109-136. DOI: 10.1016/j.pnmrs.2006.01.001.

Zhou, Y., Danbolt, N.C., 2014. Glutamate as a neurotransmitter in the healthy brain. J. Neural. Transm. 121(8), 799–817. DOI: 10.1007/s00702-014-1180-8.

10. Table

Subject	Sex	Age (months)	Age (years)	Animal rejected
283EA	M	40,8	1,3	NO
283CCA	M	41,0	1,3	NO
285AAA	M	41,3	1,4	NO
365A	M	41,3	1,4	NO
285AB	M	42,1	1,4	NO
263BCE	M	43,8	1,4	NO
314CA	M	45,0	1,5	NO
285D	M	71,2	2,3	NO
283CA	M	71,8	2,4	NO
276BC	M	72,2	2,4	NO
285E	M	72,4	2,4	NO
300BA	M	75,5	2,5	NO
289BB	F	87,0	2,9	NO
208CBF	F	95,2	3,1	NO
288BC	F	95,8	3,2	cerebral lesion
310C	F	114,8	3,8	cerebral lesion
967HACA	M	243,5	8,0	NO
184CB	F	243,6	8,0	NO
965MBIA	M	243,6	8,0	NO
965MBFA	M	244,3	8,0	NO
965MBFC	F	244,4	8,0	NO
965MBGA	M	244,7	8,0	NO
967HACB	F	244,7	8,0	NO
965MBFB	M	245,4	8,1	NO
169BAB	F	246,0	8,1	NO
965FDBB	M	265,4	8,7	NO
147BCBB	M	265,7	8,7	NO
147BCBA	M	266,3	8,8	artifact
943GKBC	F	266,5	8,8	NO
153FBA	M	311,7	10,3	NO
216B	F	317,3	10,4	NO
965MBG	F	327,7	10,8	artifact
119BBB	F	328,1	10,8	NO

Table 1. Cohort of mouse lemurs involved in the study.